

# Modeling the formation of alkali clusters attached to helium nanodroplets and the abundance of high-spin states

O. Bünermann<sup>1,a</sup> and F. Stienkemeier<sup>2</sup>

<sup>1</sup> Institut für Physikalische Chemie, Georg-August-Universität Göttingen, Tammannstr. 6, 37077 Göttingen, Germany

<sup>2</sup> Physikalisches Institut, Universität Freiburg, Hermann-Herder-Str. 3, 79104 Freiburg, Germany

Received 24 August 2010 / Received in final form 23 November 2010

Published online 25 February 2011 – © EDP Sciences, Società Italiana di Fisica, Springer-Verlag 2011

**Abstract.** The doping process of helium nanodroplets with alkali atoms has been modeled in order to study deviations from the Poissonian statistics of measured pick-up statistics which are important for assigning cluster or complex sizes in many experimental studies. Several, formally unexplained findings are reproduced and their origin has been analyzed: derivations from the expected functional form of the initial incline, the suppression of the formation of lithium clusters, the influence of the functional form and width of droplet size distributions. Furthermore, the controversially discussed formation of high-spin alkali clusters on helium droplets has been calculated within the model. The selection of high-spin states comes out to depend strongly on the experimental conditions, and is in general not pronounced for cluster sizes  $\geq 3$ . The enhancement factor of 50 of high-spin states reported in earlier experiments is reproduced when choosing the conditions of these experiments.

## 1 Introduction

The first beam of condensed helium nanodroplets was studied by Becker et al. in 1961 [1] and it took nearly 30 more years before the high potential of helium droplets for matrix isolation spectroscopy was realized. In 1990 Scheidemann et al. showed that helium nanodroplets can be loaded with neon atoms [2] and that complexes/clusters can be formed inside the droplets [3]. By now, it has become clear that helium nanodroplets provide a nearly perfect matrix for spectroscopy at temperatures of 0.37 K [4–7]. Dopants are efficiently cooled by evaporation of helium atoms off the droplets surface [8–10]. Hence, the thermal occupation of no excited vibrational and only low rotational states leads to very clean spectra. Furthermore, helium provides a very weakly perturbing environment. The droplets are superfluid [11,12] so even rotationally resolved spectra of embedded molecules have been obtained [13].

Helium nanodroplet isolation spectroscopy (HENDI) was established as a powerful tool. A vast number of atoms and molecules have been investigated by the use of HENDI, applying a variety of different experimental techniques ranging from microwave [14,15] to infrared [6] to visible [7] and even to XUV photon energies [16,17]. Because of the possibility of using helium droplets to form isolated clusters and complexes [18], cluster size-effects at cold temperatures can be studied. Due to the low temperature and rapid cooling even very fragile complexes can

be synthesized. Moreover, specific conformers like linear HCN chains [19] or high-spin alkali dimers and trimers have been aggregated in helium [20,21].

The ability to form complexes in helium droplets goes along with the disadvantage that single cluster or complex sizes cannot be selected in the doping process. The resulting distribution of different cluster sizes has hampered in many experiments the interpretation of experimental results [22–24]. In order to assign an observed spectral line to a cluster size an obvious way is the ionization and mass-selective detection of the cluster. Here, fragmentation processes are often hard to disentangle. Moreover, attached helium might mask expected dopant masses. A well established alternative is based on the pick-up statistics: helium droplets collect atoms or molecules via inelastic collisions when passing the pick-up cell. The probability to collect  $k$  particles depends on the length of the oven cell  $l$ , the cross section of the droplets  $\sigma$ , and the particle density inside the cell  $n$ . Varying the density  $n$  in the doping cell and providing  $l$  and  $\sigma$  to be constant, the abundance of every cluster size  $k$  follows the Poissonian statistics:

$$P_k(l, n, \sigma) = \frac{(ln\sigma)^k}{k!} e^{-ln\sigma}. \quad (1)$$

In the following, an intensity distribution plotted versus the particle density  $n$  will be called a doping curve. Figure 1 shows the doping curves of cluster sizes  $k = 0–5$ . The particle density is normalized based on the measured position of the maximum of the monomer curve and the experimental conditions: 10 mm length of the pick-up cell

<sup>a</sup> e-mail: oliver.buenermann@chemie.uni-goettingen.de

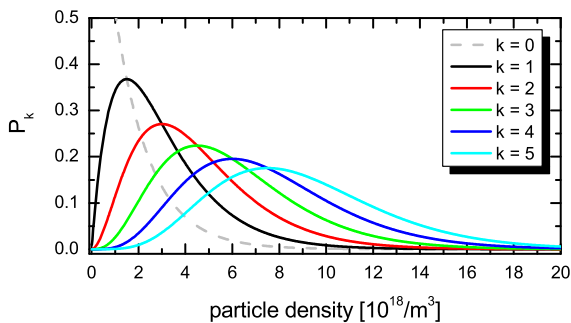


**Fig. 1.** (Color online) Theoretical doping curves according to the Poissonian statistics.

and mean droplet size of 5000. Two striking properties of these curves are immediately apparent: the maxima of different cluster sizes are equidistant;

$$n_{\max(P_k)} = \frac{k}{l\sigma}. \quad (2)$$

This allows a first guess of assigning a specific cluster size when comparing with Poissonian curves of known cluster sizes. Furthermore, the exponential function in equation (1) becomes nearly 1 for small particle densities, meaning that the initial incline follows the functional form  $n^k$ :

$$P_k(\ln\sigma \ll 1) = \frac{(\ln\sigma)^k}{k!} \propto n^k. \quad (3)$$

In several experimental studies the method of recording doping curves has been applied quite successfully in order to assign sizes of small clusters and complexes [25,26]. However, one should note that the Poissonian distributions often do not fit very well the observed doping curves. For larger complexes, the agreement is even worse. In particular clusters of alkali atoms differ strongly from the expected behavior [22,23].

Clusters of alkali atoms have received considerable interest right from the advent of cluster physics [27]. In particular the electronic and geometric structure lies in the focus of theoretical and experimental work. Over the years a large number of publications dealing with the properties of alkali clusters has been produced. The experiments showed that in particular temperature is an important parameter for the size-dependent electronic properties [28,29]. Whereas specific clusters show broad absorptions at high temperatures, absorption lines become quite narrow when clusters are cooled to 35 K. The authors predicted a  $\sqrt{T}$  law for the width of the lines. The temperature dependence of the line width can be explained as thermal average of vibrational modes when treating the clusters like having molecular transitions. Experiments with helium nanodroplet isolated clusters at 0.37 K can validate this model and have prospective options to get detailed information on the electronic structure as well as on the collective behavior of the outer electrons.

As far as the aggregation of alkali atoms on helium droplets is concerned, it is still under discussion in what spin states the resulting molecules and clusters are formed.

Experiments on dimers and trimers showed that molecules reside on the droplets' surface and molecules having all spins of the valence electrons in parallel are favored because of the much lower binding energies to be dissipated upon cluster formation [30–32]. The analysis of mass spectra of Li, Na, K, Rb and Cs clusters on helium droplets revealed that large clusters are suppressed in the case of Rb and Cs. The suppression was assigned to the instability of high-spin (HS) states because of the large spin orbit coupling. A subsequent spin flip releases a large amount of binding energy which leads to the desorption of the resulting low-spin (LS) clusters. This led the authors to the conclusion that in these experiments preferentially high-spin clusters had been formed in the size range  $<30$  [21]. However, spin statistics predicts a quite low abundance of clusters having all the spins of the valence electrons in parallel. The probability to form a HS cluster the size  $N$  out of a HS cluster of size  $N-1$  is given by:

$$P_{\text{HS}}(N-1 \rightarrow N) = \frac{N+1}{2N}. \quad (4)$$

For large  $N$  the probability converges to  $\frac{1}{2}$ , leading to a probability to form a HS cluster the size  $N$  of:

$$P_{\text{HS}}(N) \approx \frac{1}{2^N}. \quad (5)$$

Vongehr and Kresin calculated the pick-up statistics for alkali clusters predicting only high-spin clusters to remain on the droplets. Because of the limited experimental data available at that time, the resulting unusual pick-up statistics could not be confirmed nor declined by experimental data [33]. Later on, an experimental study of the formation process of rubidium dimers and trimers attached to helium droplets performed in the group of Ernst revealed [23], that the measured doping curves for high-spin formation can only for low particle densities be reproduced by the model proposed by Vongehr and Kresin. For larger particle densities the model deviates from the experiment.

In general, the question occurs how to confirm spin states and correlate electronic structure to e.g. metallic properties. Spectroscopy is a very useful tool to determine electronic structures. However, if the broadening of lines does not allow a separation of different species like it has been observed in several experiments [22,23], a selection of cluster sizes might be essential for the interpretation of experimental data. Doping curves are in that sense crucial to unravel spectra and only a detailed simulation allows a correct assignment and interpretation of the measured dependencies.

The paper is organized in the following way: after a short introduction of the experimental conditions, the model to simulate the doping process will be introduced. Then results of sodium and lithium clusters in different spin states are interpreted in comparison with experimental results.

## 2 Experiment

The setup of the molecular beam apparatus is described in detail in reference [34]. The helium droplet beam is formed by expanding high purity helium gas through a  $5\ \mu\text{m}$  nozzle into the vacuum. The source conditions of  $T_0 = 19\ \text{K}$  (temperature of the nozzle),  $p_0 = 46\ \text{bar}$  (stagnation pressure) lead to a mean droplet size of  $\bar{N} = 5000$ . For other source conditions, droplet sizes are determined using scaling laws [35].

300 mm downstream the droplets pass a 10 mm long pick-up cell containing a certain particle density of alkali atoms. The particle density can be adjusted by changing the temperature of the pick-up cell. The vapor pressure in the cell is derived from tabulated vapor pressure curves [36] which is then converted to particle density using the ideal gas law. By measuring the effusive intensity from the pick-up cell by means of Langmuir-Taylor surface ionization [37] the correct temperature dependence has been checked. In the temperature region used the portion of dimers in the vapor is 2 orders of magnitude below the monomers [38]; hence doping dimers or clusters directly from the vapor is negligible in these experiments. The doped droplet beam is ionized by a fs-laser beam inside the detection volume of a quadrupole mass-spectrometer. A Ti:sapphire oscillator having a repetition rate of 80 MHz corresponding to a pulse energy of 15 nJ and a pulse width of 110 fs was used as ionization laser. The laser was operated at a center wavelength of 760 nm = 1.63 eV resulting in  $\approx 6 \times 10^9$  photons per pulse.

The Ionization potentials of metallic bound potassium clusters are in the range of 3–3.5 eV [39], decreasing with increasing size. The photon energy provided is sufficient to ionize most of the probed clusters in a non-resonant 2 photon process, providing only a small amount of excess energy. Since the fragmentation energy of the cluster ions is in the range of 0.3–1 eV [40,41], fragmentation without thermal activation should be suppressed [42]. The dimer forms an exception having a higher IP of 4 eV. It can only be ionized in a three photon step. In the case of the weakly bound high-spin clusters a spin flip can occur releasing a large amount of binding energy which leads to fragmentation.

To illustrate the large deviations between the experiment and the Poisson statistics, Figure 2 shows the doping curves of potassium clusters up to sizes of  $k = 9$  detected mass-selectively [24]. To our knowledge this is the only available complete set of doping curves for alkali clusters larger than the trimer.

The measured doping curves cannot be explained within the Poissonian model. The maxima of the different cluster sizes are no longer equidistant but tend to group around a certain density. A large gap between the dimer and trimer mass is observed and the overall shape cannot be fitted by Poissonian curves. The monomer curve is strongly distorted by fragmentation of the high spin clusters and the effusive beam. In the result section the experimental curves will be discussed in detail in comparison to the simulated doping curves.

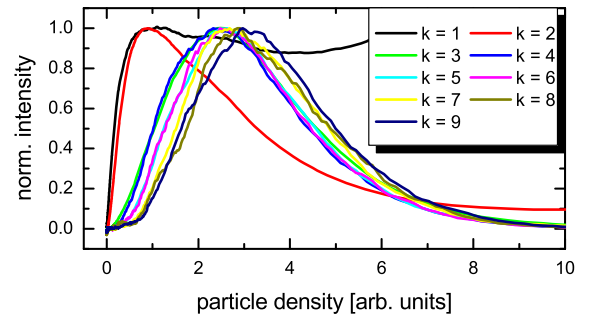


**Fig. 2.** (Color online) Doping curves of potassium clusters detected by means of multiphoton photo-ionization with a fs laser pulse [24].

## 3 Model

Helium nanodroplets have the property to collect particles by inelastic collisions with sticking probabilities close to 1. The energy carried by the dopant is transferred to the droplet and released by evaporation of helium atoms. The pick-up cross section to a good approximation is proportional to the geometric cross section of the droplets. Experimentally, the droplet beam passes a pick-up cell containing a certain particle density of atoms or molecules to collide with. By successive collisions one droplet can collect several particles which then form complexes or clusters. Changing the particle density in the cell changes the number of collisions and the average cluster size distribution on the droplets. Based on the collision probabilities and assuming that the pickup follows stochastic events with no memory between successive events, the size distributions should correspond to the Poissonian statistics.

Interpretation of intensities within the Poissonian statistics for picking up single atoms one by one during the flight through the doping cell neglects 4 important aspects:

- The droplets are produced with a wide distribution of droplets sizes.
- The droplets shrink upon every pick-up collision because of the evaporative cooling process.
- The transfer of momentum leads to a divergent droplet beam.
- Clusters bound to the surface tend to desorb upon formation because of the dissipation of binding energy.

While item one is a convolution effect, items 2 and 3 release the assumption that the process has no memory between pickup events. Item 4 describes a post pick-up behavior. All these items are modeled in the presented simulation.

### 3.1 Droplet size distribution

In the experiment the droplets are only available in size distributions. Droplet formation can be classified in three expansion regimes [4]. In the subcritical regime droplets are formed via condensation of atoms from the gas phase.

The mean droplet sizes range from a few hundreds to ten thousands of helium atoms per droplet. The size distribution follows a log-normal distribution having a width comparable to their mean size [43]. In the supercritical regime droplets are formed as fragments of the fluid. These droplets are very large having mean sizes  $2 \times 10^5$  up to  $10^7$ . The different formation process leads in this case to a size distribution, which follows a linear-exponential distribution [44]. In the critical regime a mixture of both processes takes place.

### 3.2 Droplet shrinking

Every pick-up process leads to an energy transfer to the droplets. The droplets then rapidly cool down to their terminal temperature by evaporating helium atoms. This shrinkage leads to a decrease of the scattering cross section and the probability to collect a further particle is reduced. At a certain energy entry, the complete droplet evaporates. The involved energy is composed of the following contributions:

$$E = \langle E_{\text{kin}} \rangle + E_{\text{in}} + E_{\text{binding}} + E_{\text{cluster}}. \quad (6)$$

With  $\langle E_{\text{kin}} \rangle$  the average kinetic energy,  $E_{\text{in}}$  the internal energy of the molecules,  $E_{\text{binding}}$  the binding energy of the particle to the droplet, and  $E_{\text{cluster}}$  the binding energy of the formed cluster or complex.

The average kinetic energy is given by the relative velocity of particle and droplet. Assuming a perpendicular and central collision with a much smaller mass of the particle compared to the droplet it can be estimated as:

$$\langle E_{\text{kin}} \rangle \approx \frac{3}{2} k_B T + \frac{1}{2} m_{\text{particle}} v_{\text{droplet}}^2 \quad (7)$$

where  $T$  denotes the temperature in the pick-up cell. In the case of atoms, the internal energy is 0; but even small molecules can carry a significant amount of energy to be considered. In contrast to most atoms and molecules, the binding energy of alkali atoms to the droplet is only in the order of  $10 \text{ cm}^{-1}$  [45]. The binding energy (BE) of the formed alkali clusters is strongly dependent on their spin configuration. A high-spin (HS) cluster, where all spins are in parallel, has a much lower BE than a cluster in a singlet/doublet state, where pairing of antiparallel spins increases the binding properties of the valence electrons. This energy, again, has to be dissipated by evaporating helium atoms which are bound to the droplet by  $5 \text{ cm}^{-1}$  [46]. Lehmann and Dokter developed a model for the evaporative cooling of helium nanodroplets including angular momentum conservation [10]. The calculations predict that depending on the initial angular momentum of the droplet one He atom carries additional energy of up to  $3 \text{ cm}^{-1}$  which would lead to a reduced shrinking in our model. During this process the droplet shrinks and its cross section is reduced. As an example, the pick-up of one Na atom leads to an evaporation of approximately 100 helium atoms, the pick-up of a  $\text{SF}_6$  molecule to the evaporation of around 500 atoms.

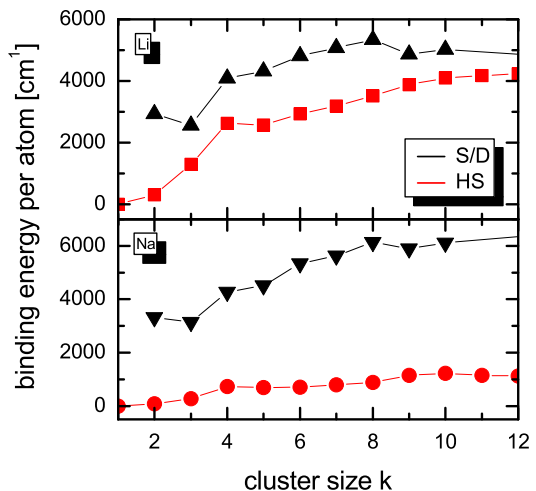


**Fig. 3.** (Color online) Calculated binding energies of Na and Li clusters in different spin states [47–49]. S/D: singlet /doublet states, HS: high-spin state having all spins of the valence electrons in parallel.

The size of the clusters is limited by the maximum energy the droplets can dissipate. As the experimental studies have shown, the droplets act as a filter for weakly bound complexes [4]. For example, in the formation of alkali trimers the quartet states were very much enhanced compared to the doublet trimers. Figure 3 shows the binding energies of lithium and sodium clusters up to a size of 12 in different spin configurations [47–49]. In the case of sodium the differences between the HS and doublet/singlet states are considerable, whereas in the case of lithium the difference is only moderate. The difference between lithium and the other alkalis is associated to a different ordering of the molecular orbitals due to a shorter bond length, leading to a significant ferro magnetic binding energy [47]. The binding energy of a HS sodium trimer leads to the evaporation of 160 atoms but the binding energy of the doublet trimer to an evaporation of 1900 atoms. In our simulation we will classify results to their overall spin state: HS indicating the clusters with all spins parallel, low spin LS all other configurations.

### 3.3 Momentum transfer

In addition to energy, also momentum is transferred to the droplets during the doping process. Because of the much higher mass of the droplets this momentum can be neglected for weak doping. However, if several atoms are collected, the momentum transfer leads to a considerable spatially diverging beam. In general, one only has a small interaction region, for example, given by the diameter of a laser beam. The increased divergence of the beam therefore leads to droplets missing the detector and consequently results in a decrease of the recorded signal. The simulation revealed that the momentum distribution of droplets follows a 3D normal distribution after passing the oven cell. The effect of the momentum transfer

is strongly depended on the geometry of the experiment. The longer the distance between pick-up and interaction region and the smaller the interaction region, the bigger this influence is.

### 3.4 Cluster desorption

Another characteristic of alkali atoms and clusters is their ability not to solvate inside the droplet but to reside in a dimple on the surface. Since the binding energy of the formed cluster which is dissipated upon cluster formation is much higher compared to the binding energy to the droplet surface, desorption off the droplet's surface is a prominent process. In order to describe the desorption process we tested three different models and compared the resulting doping curves with the experimentally observed ones.

1. In the first model the cluster always desorbs when the released energy exceeds a fixed value. This model corresponds to the process Vongehr and Kresin proposed [33]. The value of the threshold is chosen in a way that LS clusters always desorb and HS clusters never.
2. In the second model the desorption probability is proportional to the ratio of the released energy and the total energy of the droplet, making the desorption dependent on the droplet size.
3. In the third model the desorption probability is proportional to the ratio of the released energy and the binding energy of all helium atoms located at the surface of the droplet. This is based on the idea, that the desorption of helium atoms is isotropic and the cluster will desorb if the outer helium shell desorbs.

The third model showed the best agreement with the experiment and was used in the simulations presented here.

Clusters with exceptionally high binding energy per atom are strongly suppressed by the desorption model and so are the cluster sizes building on that cluster. Additionally, droplets can be doped again after having released clusters. This leads to an increase of the abundance of small clusters at high particle densities.

### 3.5 Simulation procedure

The modeling is based on a numerical simulation of droplets of a certain size and velocity picking up a certain number of dopand particles carrying thermal energy and momentum. A 4-dimensional  $N \times M \times k \times S$  matrix is constructed where  $N$  represents the droplet size,  $M$  the number of collisions of the droplet,  $k$  the doped cluster size, and  $S$  the spin state of the doped cluster. We start with a size distribution of droplets corresponding to the experimental conditions. The droplets pass the "oven cell" of length  $l$  stepwise. The steps  $dl$  are chosen in a way that the probability to collect two particles is much smaller than only collecting one according to the Poissonian distribution. So we can neglect  $P_{k>1}(dl, \sigma, n)$ . For each step

the probability to collect one atom, droplet shrinking and the desorption probability are calculated and applied to the matrix. After passing the cell the correction from picking up momentum is computed.

As a result we obtain the probabilities having droplets of size  $N$  which have undergone  $M$  collisions, doped with a cluster of size  $k$  in spin state  $S$ . Integrating over  $N$  and  $M$  calculates for each density  $n$  the doping curve.

## 4 Results

In this article we present the simulation of sodium and lithium clusters with different droplet beam and oven cell conditions. For potassium, rubidium and cesium clusters there is no spin-dependent set of binding energies available. However, in the case of potassium a very similar behavior when compared to sodium is expected, since the binding energies of the clusters are comparable in the LS case [50]. Moreover, the mass spectra of sodium and potassium clusters embedded in helium nanodroplets have been measured to generate very similar size distributions [21] which underlines a comparable doping scenario. From the experimental point only for potassium a complete set of doping curves has been measured. Concerning the characteristics of the droplet beam, parameters according to our experimental conditions were used. Mostly we carried out experiments in the subcritical regime of droplet formation because of the high density of produced droplets. Typical droplet sizes are in the region of 5000–20000 helium atoms. In the subcritical regime the velocity  $v$  of the beam can be calculated by [51]:

$$v = \sqrt{2h(T_0, p_0)} \quad (8)$$

with  $h(T_0, p_0)$  the real gas enthalpy per unit mass at stagnation conditions  $T_0$  and  $p_0$ . In the supercritical regime it is proportional to  $\sqrt{T_0}$  [51].

The simulation models the experimental conditions of our apparatus: our oven cells have a length of 10 mm, the distance to the interaction zone is 300 mm and its diameter is 1 mm. The corresponding parameters were scaled in a way, that the maximum of the simulated doping curve for the sodium monomer matches the measured one, which is located at a sodium vapor pressure of  $10^{-4}$  mbar ( $n = 1.6 \times 10^{18}/\text{m}^3$ ) in the oven cell and for a mean droplet size of 5000.

As an example, Figure 4 plots the result for a sodium trimer in the high-spin state, formed in a droplet beam with a mean size of 5000 and FWHM of 4000. The false color picture shows the probability to find the trimer on a specific droplet size as a function of the particle density  $n$  in the oven cell. The bottom bar represents the droplet size distribution prior to doping. The black line marks the mean droplet size of the actual size distribution. At low particle densities (below the maximum of the left panel in Fig. 4) the mean droplet size given by the black line is shifted to higher  $N$  when compared to the mean of the initial droplet size distribution. In this region very large droplets significantly contribute because the smaller

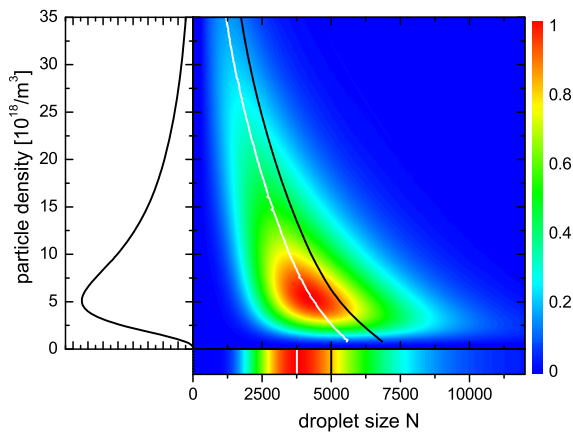


**Fig. 4.** (Color online) Probability of finding a sodium trimer in a droplet of size  $N$  dependent on the density of atoms in the pick-up cell. Droplets were assumed to initially have a log-normal distribution with a mean size of 5000, which is represented by the bar on the bottom. The left panel plots the  $\text{Na}_3$  intensity integrated over all droplet sizes. The black line indicates the mean droplet size  $N$  the white line the maximum of the distribution.

droplets have a low probability to collect three atoms. At conditions corresponding to the maximum of the simulated doping curve the size distribution is very similar to the original one, being shifted only a little bit to larger  $N$ . Carrying out the integral over  $N$  results in the doping curve shown to the left.

The simulation shows that the mean droplet size for maximum doping conditions of that specific cluster size is very similar to the undoped situation. To illustrate the important trends, Figure 5 shows the influence of cluster size, spin state and particle density on the underlying droplet size distributions. The black lines mark the maximum of the doping curves. The larger the cluster the more the underlying droplet size distribution is shifted to larger droplet sizes. For complexes with an exceptionally high binding energy this effect can be very pronounced. For example, the singlet dimer is carried by droplets having a mean droplet size of  $\approx 8000$ , nearly twice the original one. The size distribution of the doped droplets changes with the doping conditions, beginning with a large mean size for low particle density which decreases with increasing particle density.

In many published results only the undoped cluster sizes are given. One has to note here that the doped droplet size can significantly deviate, depending on the doping conditions. Moreover, the evolution of the distributions with increasing cluster size is opposite to what one would naively expect. The mean droplet size for larger clusters is larger than the one for smaller ones. The reason for this is, that for larger clusters only a small portion of the droplets is able to carry the cluster into the detection volume, cutting off a part of the underlying distribution.

The simulation allows to isolate the influence of the four incorporated effects discussed in Section 3. Taking into account the droplet size distributions leads to an

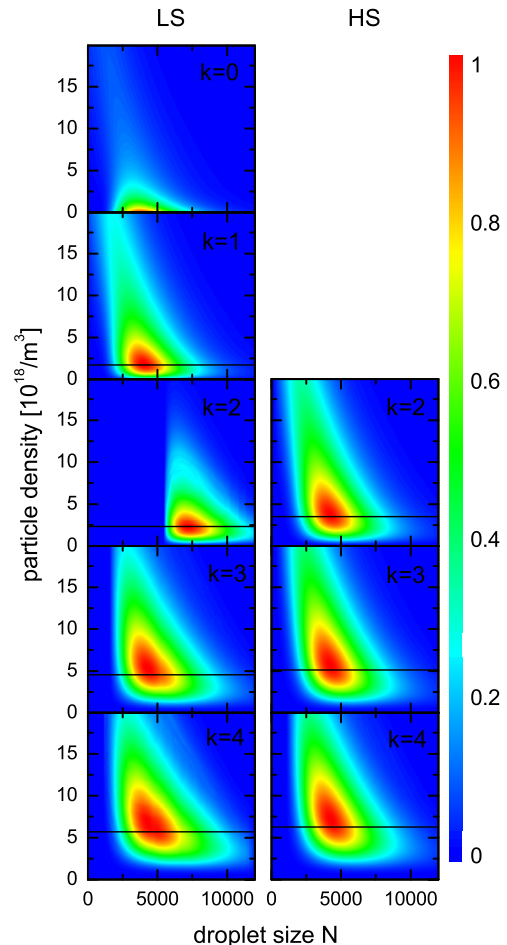


**Fig. 5.** (Color online) Probability of finding a sodium cluster of size  $k$  in the HS or LS state in a droplet of size  $N$  dependent on the density of atoms in the pick-up cell. The black lines mark the maximum of the simulated doping curve. Droplets were assumed to initially have a log-normal distribution with a mean size of 5000.

overall broadening of the doping curves. The simulations show that this broadening is the main reason for the observed exponents being too small in the initial incline of the doping curves. Additionally, the tail of the size distribution enables the formation of very large clusters. Droplet shrinking and desorption lower the probability to form large clusters. Additionally, the desorption model favors clusters with low binding energy. The momentum transfer strongly influences the doping process at high particle density leading, in general, to a decrease in the number of formed clusters.

#### 4.1 Subcritical expansion regime

In the subcritical regime the droplet size distribution follows a log-normal distribution. Typical droplet sizes used in the experiments are in the range of 5000–20000. The simulation was carried out for sodium and lithium. The results are qualitatively similar so we will concentrate the

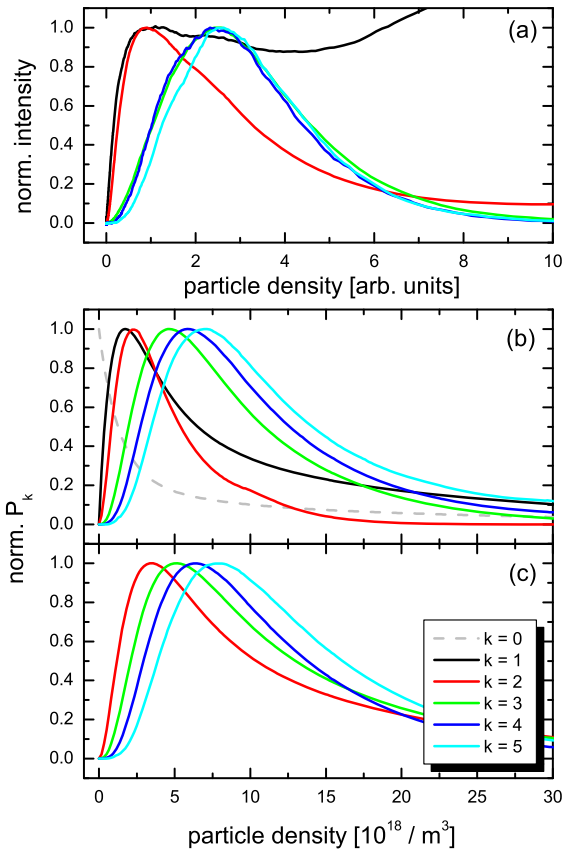


**Fig. 6.** (Color online) (a) Experimentally measured doping curves of potassium clusters. (b) Simulated doping curve for Na LS clusters. (c) Simulated doping curve for Na HS clusters.

discussion on sodium. However, we have to point out once again, that lithium is special in the line of alkali atoms, showing much less dependence in the binding energies on the spin state.

### Sodium clusters

Figure 6 shows experimentally observed doping curves of small potassium clusters (graph (a)) in comparison to the simulated curves for sodium clusters for droplet condition  $\bar{N} = 5000, N_{1/2} = 4000$ . Graph (b) shows the results of clusters in the LS states, (c) the one for the HS ones. In particular the doping curves for LS clusters differ strongly from the Poisson statistic (cf. Fig. 1). In contrast to the Poissonian curves, a notable part ( $\sim 10\%$ ) of the droplets remain undoped (Fig. 6–graph (b)).

The monomer and dimer maxima almost overlap and are quite separated from the maxima of larger clusters which group together at higher particle densities. This behavior nicely meets the observations. The HS clusters do not group, but have roughly equidistant maxima like the Poissonian curves. This already indicates that under these conditions high-spin clusters are not preferentially detected. This issue will be discussed later. When comparing the simulation with the experiment we have to keep

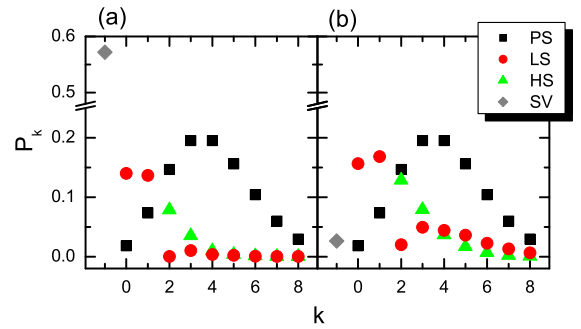


**Fig. 7.** (Color online) Cluster size distribution for conditions leading to a maximum of the tetramer signal for initial droplet size distributions with a mean size of (a) 5000 and (b) 20000. PS = Poisson statistic, LS = low spin clusters, HS = high-spin clusters, SV = scattered or vaporized droplets.

in mind, that fragmentation upon detection leads to cross talk of the different masses in the experimental data. This can e.g. be seen on the monomer and dimer mass, where we get a contribution of the higher masses when going to heavy doping (Fig. 6a). Such fragmentation has not been included in the presented simulation since we are interested in the cluster size distribution after the pick up process. The amount of fragmentation will be discussed below.

The increase of the monomer curve to very high vapor pressures stems from background atoms, coming from the effusive beam of the very hot oven cell.

HS clusters have a much larger tendency to fragment, because upon ionization a spin flip is likely, releasing a huge amount of binding energy [52,53]. In most cases monomer fragments will appear and contribute to the monomer doping curve. Following this line of interpretation large HS clusters should not contribute to the doping curves recorded on their parent masses but to the doping curves of the corresponding fragments masses. However, the LS clusters do not tend to fragment and contribute to the doping curve of their parent masses. This behavior is observed in the experiment. The doping curves of potassium clusters larger than  $k = 2$  (Fig. 6) are best modeled by LS clusters. The monomer and dimer curves reveal a large contribution of fragmentation from higher masses, most likely HS clusters.

In Figure 6 the curves are normalized to allow a better comparison. However, also the absolute amplitude of the curves is of interest. The simulation revealed that in general the number of droplets carrying a cluster of specific size is less than we expect in the case of Poissonian curves. Here also the droplet size plays an important role.

The complete cluster size distribution for conditions leading to a maximum of formed tetramers is shown in Figure 7 for two different mean droplet sizes. For comparison the distribution expected from Poissonian statistics is also included. In case of a mean droplet size of 5000, most of the droplets either carry no cluster when leaving the doping region or do not reach the detection volume. Almost 60% do not reach the detector; either because they have completely evaporated or have been scattered off the

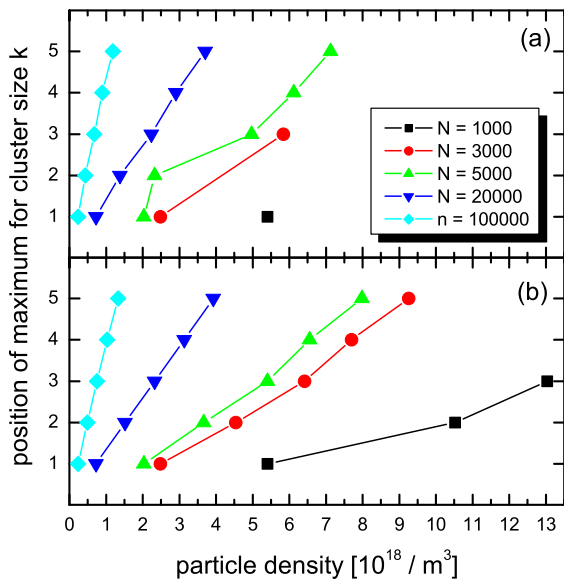


**Fig. 8.** (Color online) Position of the maxima of the simulated doping curves as a function of the mean droplet size  $N$ . (a) LS clusters, (b) HS clusters.

acceptance region because of high momentum transfer. 15% of the droplets carry no clusters. Cluster sizes larger than 3 are strongly suppressed, the tetramer only has a probability of  $<1\%$ . Increasing the droplet size leads to a different picture. Only a small amount of droplets is scattered or evaporates. Still most of the droplets carry monomers or dimers and even the large clusters are abundant with notable contribution. Adding the probabilities of LS and HS clusters give a quite similar picture compared to the Poissonian statistic, only shifted to smaller sizes.

Comparing the described distributions with experimental results [5] is not straight forward. The experimental mass spectra are characterized by shell structures pointing to fragmentation patterns. Hence they do not represent the genuine distribution of clusters on the droplets. However, as discussed later, fragmentation upon detection does not severely scramble the assignment of cluster sizes. The measured mass spectra as the simulated ones show a strong decrease of larger clusters, even for intense doping. In order to observe larger clusters at all, large droplet sizes are required.

For a detailed analysis the simulation was done for several mean cluster sizes. Figure 8 shows the position of the maxima of the simulated doping curves for different cluster sizes  $k$ . Graph (a) shows the position of the LS clusters and (b) the position of high-spins. Droplets of a small average size cannot dissipate much energy and the cluster size distribution is cut off very early. E.g., droplets of sizes less than 3000 completely evaporate when the binding energy of a singlet dimer is dissipated into the droplet; hence singlet dimers are completely missing in Figure 8. The HS clusters also stop at a size of 3 at this droplet size.

For the HS clusters the maxima are roughly equidistant. The LS clusters show the already mentioned

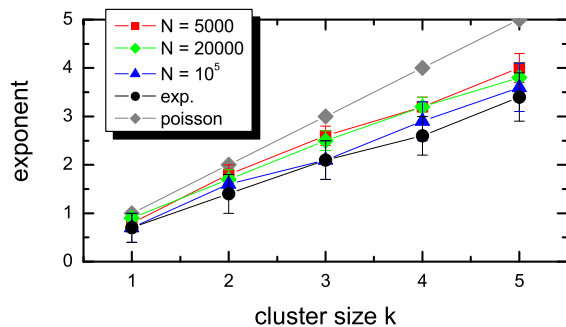


**Fig. 9.** (Color online) Exponent of the rise of the simulated doping curves for sodium in comparison with the Poissonian statistics and the experimental values.

grouping for droplet sizes in the range of 5000. This is caused by the very high binding energy of the singlet dimer and leads to high desorption probabilities upon formation. Singlet dimers only stay on very large droplets. This has the effect that only a small part of the droplet size distribution is doped. These are the large droplets having large scattering cross sections. Therefore the doping curve is shifted to lower particle densities. The LS clusters from size 3 on are mainly formed from triplet dimers, leading to the gap between dimer and trimer. At very large cluster sizes, the singlet dimer stays on the droplet and the gap separating the larger clusters disappears. This means, that the positions of the maxima are significantly effected by the desorption and shrinking model.

One can also analyze the initial incline of the curves by fitting them to polynomials. The curvature should be proportional  $n^k$ . Surprisingly, the experiment revealed, that the exponents are smaller than the expected  $k$ , still being equidistant. First of all this confirms that in our experiments the clusters are not detected to a large extend on fragment masses, since this would result in too *large* exponents. Hence, fragmentation upon detection does not contribute significantly. The experimental curves as well as the simulated ones cannot be fitted very well with a Poissonian curve. In particular for heavy doping (higher densities) deviations are severe. In order to obtain the exponents of the initial part we fit only up to the maximum. The resulting exponents for the simulation are shown in Figure 9 in comparison to experimental values. The simulation clearly confirms the too small exponents, like observed in the experiment. It appears that the larger the mean droplet size, the more the exponents decrease. Here, the increased widths of the size distributions of larger droplets is responsible for the decrease of the exponent. This opens up the possibility to use Poissonian curves to determine the widths of size distributions of droplet sources.

In the following the formation of high-spin clusters and in particular the ratio of HS to LS clusters has to be discussed further. A ratio of singlet to triplet dimers of 1:50 was observed experimentally [20]. Only looking at the spin statistics, a ratio of 1:3 is expected. Figure 10 plots the ratio for the different simulated mean droplet sizes. For a mean droplet size of 100 000 and 20 000 respectively, the

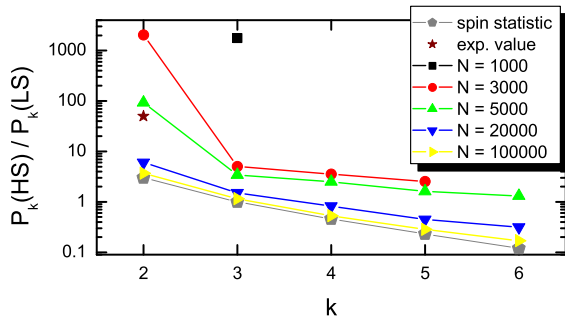


**Fig. 10.** (Color online) Ratio of HS to LS clusters in dependence of the cluster size  $k$  and the mean droplet size  $\bar{N}$ . Additionally the expected ratio based on spin statistics as well as an experimental value [20] is included in the figure.

ratios of the different cluster sizes are close to the ones expected by theory. However, for smaller droplets the HS clusters more and more dominate and one can choose experimental conditions where even for tetramers and larger clusters the low spin species are significantly suppressed. For a mean droplet size of 5000 the dimers have a ratio of 1:90, meaning the experimental observed ratio is reached at a mean droplet size between 5000 and 20000 atoms, reflecting well the experimental conditions. In conclusion, depending on the experimental conditions, high-spin clusters can be selected during the doping process; however, for large droplet sizes this enhancement effect disappears.

### Lithium clusters

Similar simulations have also been carried out for lithium clusters. The main difference between lithium and sodium are the binding energies of the clusters (Fig. 3). While in the case of sodium the binding energy of the singlet/doublet configurations are much higher compared to the HS clusters, in the case of lithium the difference is quite moderate. Only the triplet dimer has a much smaller binding energy than the singlet state. In particular, the HS trimer and HS tetramer have a quite high binding energy. In view of our simulation it is now quite obvious that during the earlier experiments [21] no larger lithium clusters have been observed. Clusters larger than the trimer are strongly suppressed in the simulations. Again the suppression of large clusters disappears when increasing mean droplet sizes.

### 4.2 Supercritical regime

In order to form clusters much larger than 10 very large droplet sizes are required. In the subcritical expansion regime the mean size will not exceed a few ten thousand atoms but in the supercritical regime droplets containing millions of helium atoms can easily be produced. Because of the different droplet formation process a completely different droplet size distribution is present, now following a linear-exponential function. Like already discussed,

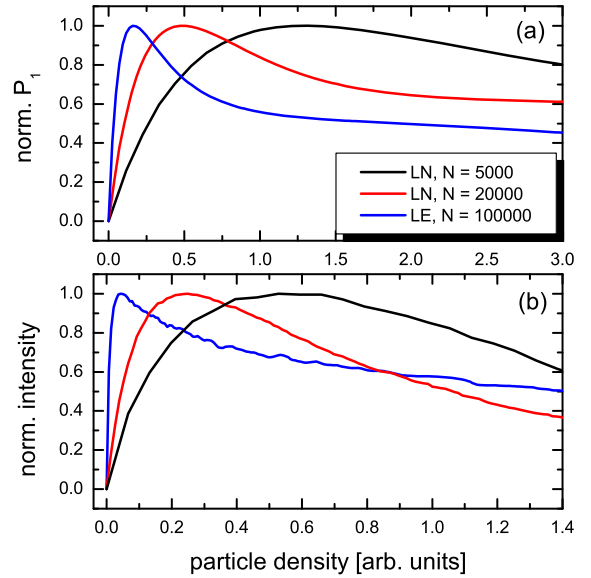


**Fig. 11.** (Color online) Doping curves for the Li monomer as a function of the mean droplet size. (a) Simulation, (b) experiment, LN = log normal, LE = linear exponential.

a change of the size distribution will also change the doping curves. This has to be accounted for when analyzing the size of the clusters via doping curves.

Figure 11 shows experimental doping curves for the lithium monomers as a function of the mean droplet size in comparison to the calculated doping curves. The change of the curve with the droplet distribution can be modeled well by the simulation. Going to larger  $N$  leads to a shift of the maximum to lower particle densities. Also the change in the slope when reaching the supercritical regime is reproduced. This clearly indicates that the distribution of droplet sizes, which can significantly vary depending on the source conditions, has to be considered when fitting and analyzing doping curves.

## 5 Conclusion

The simulations presented in this article are well suited to reproduce the experimentally observed doping curves for small alkali clusters. The discrepancies between the Poissonian statistics and the observed experimental curves can be explained and attributed to different effects of the doping process. The simulation confirms the experimental observation, that it is difficult to assign a defined cluster size to an observed cluster only by recording the doping curve, at least for sizes larger than 3. Increasing the mean size of the droplets can significantly but not completely reduce this problem.

In detail, the too small exponents can be explained within the simulation and are attributed to the underlying droplet size distribution. Furthermore, the shape of the doping curves is strongly influenced by the droplet size distribution. Droplet shrinking and cluster desorption lead to intuitively unexpected shifts of the doping curves.

Cluster with exceptional large binding energies are more abundant at lower particle densities since only very large droplets can absorb the released binding energy. For heavy doping one has to consider momentum transfer to suppress the formation of small clusters.

A further important result is, that for large alkali clusters HS states like proposed in reference [21] are only produced at very special experimental conditions and not a general feature. For small cluster sizes (dimers, trimers) the simulation revealed that high-spin molecules are favored, like observed in several experiments. When the droplet size is large enough this effect is less pronounced and it is possible to form low spin entities. The experimental observed ratio of singlet to triplet dimers of 1:50 [20] is reproduced for the conditions of these experiments.

Looking at the heavier alkali atoms, for potassium the same behavior as for sodium is expected. In the case of rubidium and cesium former experiments revealed that large clusters cannot be formed. The lack of large clusters was explained by the instability of the high-spin clusters due to the large spin orbit coupling [21]. The simulation points to an alternative explanation. Due to the larger mass of rubidium and cesium the momentum transfer could be responsible for the absence of large clusters. In recent experiments performed in our laboratories we were able to observe larger clusters when using much larger helium droplets. Again this represents very well the results of the simulations.

Simulations can easily be extended to complexes other than alkalis. However, the peculiar situation of the weak binding and surface location of alkalis on helium droplets amplifies many effects and results in most drastic deviations from statistical behavior for these systems of alkali atoms. Apart from the desorption mechanism, all other effects also apply to dopands which are solvated inside helium droplets. One important result which can be transferred to any system is that the size distribution of the droplets has a large influence on the doping curves. Especially concerning large clusters or complexes the doping curves differ strongly from the Poissonian statistics.

Finally, the simulations have been used to test different oven configurations in order to check effects on the length of the doping region. Except for shifts of the doping curves, no big difference could be found when changing the length of the oven cell. This might be evident, because the main energy transferred to the droplet results from the cluster's binding energies and not from the kinetic energy which is the only parameter that changes. The same is true for different droplet beam velocities.

In conclusion, the simulations clearly point out that the analysis of doping curves can exhibit surprising results like e.g. too small exponents of the initial incline or drastic effects when changing helium droplet size distributions. In general these effects are well reproduced in the simulations. However, one has to be careful when using doping curves to assign sizes of clusters and complexes because the experimental conditions strongly determine the outcome of the measured curves.

Financial support of this work by the Deutsche Forschungsgemeinschaft is gratefully acknowledged.

## References

1. E.W. Becker, R. Klingelhöfer, P. Lohse, *Zeitschrift Naturforschung* **16**, 1259 (1961)
2. A. Scheidemann, J.P. Toennies, J.A. Northby, *Phys. Rev. Lett.* **64**, 1899 (1990)
3. M. Lewerenz, B. Schilling, J.P. Toennies, *J. Chem. Phys.* **102**, 8191 (1995)
4. J.P. Toennies, A.F. Vilesov, *Angew. Chem. Ind. Ed.* **43**, 2622 (2004)
5. J. Tiggesbäumker, F. Stienkemeier, *Phys. Chem. Chem. Phys.* **9**, 4748 (2007)
6. C. Callegari, K.K. Lehmann, R. Schmied, G. Scoles, *J. Chem. Phys.* **115**, 10090 (2001)
7. F. Stienkemeier, A.F. Vilesov, *J. Chem. Phys.* **115**, 10119 (2001)
8. M. Hartmann, R.E. Miller, J.P. Toennies, A. Vilesov, *Phys. Rev. Lett.* **75**, 1566 (1995)
9. D.M. Brink, S. Stringari, *Z. Phys. D* **15**, 257 (1990)
10. K.K. Lehmann, A.M. Dokter, *Phys. Rev. Lett.* **92**, 173401 (2004)
11. M. Hartmann, F. Mielke, J.P. Toennies, A.F. Vilesov, *Phys. Rev. Lett.* **76**, 4560 (1996)
12. S. Grebenev, J.P. Toennies, A.F. Vilesov, *Science* **279**, 2083 (1998)
13. R. Fröchtenicht, J.P. Toennies, A. Vilesov, *Chem. Phys. Lett.* **229**, 1 (1994)
14. I. Reinhard, C. Callegari, A. Conjusteau, K.K. Lehmann, G. Scoles, *Phys. Rev. Lett.* **82**, 5036 (1999)
15. C. Callegari, I. Reinhard, K.K. Lehmann, G. Scoles, K. Nauta, R.E. Miller, *J. Chem. Phys.* **113**, 4636 (2000)
16. K. von Haefen, T. Laarmann, H. Wabnitz, T. Möller, *Phys. Rev. Lett.* **87**, 153403 (2001)
17. D.S. Peterka, J.H. Kim, C.C. Wang, L. Poisson, D.M. Neumark, *J. Phys. Chem. A* **111**, 7449 (2007)
18. J. Tiggesbäumker, F. Stienkemeier, *Phys. Chem. Chem. Phys.* **9**, 4748 (2007)
19. K. Nauta, R.E. Miller, *Science* **283**, 1895 (1999)
20. F. Stienkemeier, J. Higgins, W.E. Ernst, G. Scoles, *Phys. Rev. Lett.* **74**, 3592 (1995)
21. C.P. Schulz, P. Claas, D. Schumacher, F. Stienkemeier, *Phys. Rev. Lett.* **92**, 013401 (2004)
22. O. Bünermann, M. Mudrich, M. Weidemüller, F. Stienkemeier, *J. Chem. Phys.* **121**, 8880 (2004)
23. J. Nagl, G. Auböck, A.W. Hauser, O. Allard, C. Callegari, W.E. Ernst, *J. Chem. Phys.* **128**, 154320 (2008)
24. P. Claas, Ph.D. thesis, University of Bielefeld, 2006
25. M. Hartmann, R.E. Miller, J.P. Toennies, A.F. Vilesov, *Science* **272**, 1631 (1996)
26. M. Wewer, F. Stienkemeier, *Phys. Rev. B* **67**, 125201 (2003)
27. W.A. de Herr, *Rev. Mod. Phys.* **65**, 611 (1993)
28. C. Ellert, M. Schmidt, C. Schmitt, T. Reiners, H. Haberland, *Phys. Rev. Lett.* **75**, 1731 (1995)
29. M. Schmidt, C. Ellert, W. Kronmüller, H. Haberland, *Phys. Rev. B* **59**, 10970 (1999)

30. F. Stienkemeier, W.E. Ernst, J. Higgins, G. Scoles, J. Chem. Phys. **102**, 615 (1995)
31. J. Higgins, C. Callegari, J. Reho, F. Stienkemeier, W.E. Ernst, K.K. Lehmann, M. Gutowski, G. Scoles, Science **273**, 629 (1996)
32. J. Higgins, C. Callegari, J. Reho, F. Stienkemeier, W.E. Ernst, G. Scoles, J. Phys. Chem. A **102**, 4952 (1998)
33. S. Vongehr, V.V. Kresin, J. Chem. Phys. **119**, 11124 (2003)
34. P. Claas, G. Droppelmann, C.P. Schulz, M. Mudrich, F. Stienkemeier, J. Phys. B At. Mol. Opt. Phys. **39**, S1151 (2006)
35. H. Haberland, in *Clusters of Atoms and Molecules*, edited by H. Haberland (Springer-Verlag, Berlin, 1995)
36. D.R. Lide. *CRC handbook of chemistry and physics* (CRC Press, 2005)
37. F. Stienkemeier, M. Wewer, F. Meier, H.O. Lutz, Rev. Sci. Instrum. **71**, 3480 (2000)
38. M. Makansi, W.A. Sleke, C.F. Bonilla, J. Chem. Eng. Data **5**, 441 (1960)
39. C. Bréchnignac, in *Clusters of Atoms and Molecules*, edited by H. Haberland (Springer-Verlag, Berlin, 1995)
40. C. Bréchnignac, Ph. Cahuzac, F. Carlier, M. de Frutos, J. Leygnier, J. Chem. Phys. **93**, 7449 (1990)
41. F. Spiegelmann, D. Pavolini, J. Chem. Phys. **89**, 4954 (1988)
42. I.V. Hertel, C.P. Schulz, A. Goerke, H. Palm, G. Leipelt, J. Chem. Phys. **107**, 3528 (1997)
43. J. Harms, J.P. Toennies, F. Dalfovo, Phys. Rev. B **58**, 3341 (1998)
44. E.L. Knuth, U. Henne, J. Chem. Phys. **110**, 2664 (1999)
45. F. Ancilotto, G. DeTofol, F. Toigo, Phys. Rev. B **52**, 16125 (1995)
46. S. Stringari, J. Treiner, J. Chem. Phys. **87**, 5021 (1987)
47. S.P. de Visser, D. Danovich, S. Shaik, Phys. Chem. Chem. Phys. **5**, 158 (2003)
48. I. Boustani, W. Pewestorf, P. Fantucci, V. Bonačić-Koutecký, J. Koutecký, Phys. Rev. B **35**, 9437 (1987)
49. U. Röthlisberger, W. Andreoni, J. Chem. Phys. **94**, 8129 (1991)
50. A. Banerjee, T.K. Ghanty, A. Chakrabarti, J. Phys. Chem. A **112**, 12303 (2008)
51. H. Buchenau, E.L. Knuth, J. Northby, J.P. Toennies, C. Winkler, J. Chem. Phys. **92**, 6875 (1990)
52. J.H. Reho, J. Higgins, M. Nooijen, K.K. Lehmann, G. Scoles, J. Chem. Phys. **115**, 10265 (2001)
53. J.H. Reho, J.P. Higgins, K.K. Lehmann, Faraday Disc. **118**, 33 (2001)